Evaluation of Adsorption Kinetic of Chromium (VI) Using N-doped Carbon Based on Palm Empty Fruit Bunches

Susanto Susanto[1], Moch. Agung Indra Iswara[1], Ulfiana Ihda Afifa[1], and Khalimatus Sa'diyah[1]

[1] Department of Chemical Engineering, State Polytechnic of Malang, Jl. Soekarno-Hatta No. 9, Malang 65141, Indonesia

Abstract. Chromium (Cr) is a heavy metal widely used in various industries. Chromium (Cr), a heavy metal, has significant risks to human health and the environment. Chromium in the hexavalent form (Cr VI) is more hazardous than chromium in the trivalent form (Cr III). This work investigated the performance of N-doped carbon derived from palm empty fruit bunches for adsorbing hexavalent chromium (Cr VI) from an aqueous solution, and it also investigated the kinetics of adsorption. N-doped carbon is synthesized via the preparation of cellulose aerogels derived from palm empty fruit bunches, utilizing a crosslinking agent comprising ammonia, urea, and NaOH solution, followed by pyrolysis and adsorption performance evaluations on 100 ppm of Cr(VI) metal at various contact times (15, 30, 45, 60, 90, 120 min). N-doped carbon has been successfully produced from cellulose aerogel based on palm empty fruit bunches, exhibiting a nitrogen doping level of 13% and a high specific surface area. N-doped carbon containing pyridinic nitrogen is capable of absorbing Cr(VI) metal ions with a capacity of 126.05 mg/g, achieving optimal adsorption within 30 minutes at an initial concentration of 100 ppm of the adsorbate. At pH 6, the adsorption of doped carbon N, featuring a pyridinic active group N that is protonated into pyridinium species, occurs with the metal ion Cr (VI) in the form of $(CrO_4)^{2-}$. This process involves chemical interactions that can be categorized as electrostatic interactions, and the kinetics of the reaction follows a pseudo second order, exhibiting an R^2 value of 0.99715.

Keywords: Adsorption kinetics, Chromium (VI), N-doped carbon, Pyridinic N.

1. Introduction

Chromium (Cr) is a heavy metal widely used in the tanning industry, metallurgy, electroplating, dye colors, and batteries [1–6]. Chromium, a heavy metal, causes several significant hazards to human health and the environment [4,7]. Metal Cr(VI) is 100 times more hazardous than metal Cr(III) due to its higher toxicity, oxidation potential, solubility, and bioavailability [4,8–11]. Cr(VI) metal ions that associate with oxygen can easily diffuse in the environment and into the human body via the food chain [12].

S. C. Asih et al. (eds.), *Proceedings of the 19th International Conference on Quality in Research (QiR 2025)*, Advances in Engineering Research 303,
https://doi.org/10.2991/978-94-6239-717-0_19

Chromium (VI) is linked with cancer risk, internal organ damage, and skin and respiratory issues, along with genotoxic and immunotoxic effects [4,8,9,13]. The permitted limit for Cr(VI) in industrial wastewater is set at 0.5 mg/L [10]. The World Health Organization states that the highest permitted total chromium concentration in drinking water is 0.05 mg/L [6,10,14]. The metal ion Cr (VI) exists in water in several forms of ion species, including CrO_4^{2-}, $Cr_2O_7^{2-}$, and $HCrO_4^-$ [15]. Chromium (VI) stands out as a critical focus in the treatment of heavy metal contamination in the environment.

Technologies for the treatment of heavy metal waste, specifically for Cr(VI), consist of adsorption, electrodeposition, membrane filtration, flotation, ion exchange, and photocatalytic reduction [8,16,17]. Adsorption has several benefits especially the utilization of easy equipment, low-cost, and the capability apply adsorbents with modified functional groups [18–23]. Adsorbents contain active groups such as hydroxyl (OH), mercaptan (SH), and amine (N-H) groups [18,24]. N-doped carbon containing amine groups can be used as an adsorbent for Cr(VI) metal [25,26]. The amine reagents researched on N-doped carbon are derived from piperazine, m-phenylenediamine, and melamine, noted for their high costs and unenvironmentally friendly [14,15,27–29]. Alternatively, a precursor mixture of urea solution can be used with lower cost and more environmentally friendly [30–32]. Zhao et al. have synthesized N-doped carbon from commercial cellulose using urea as the N-doping source via the hydrothermal technique, achieving an adsorption capacity for Cr (VI) of 151 mg/g [12]. Furthermore, cellulose is commonly utilized as a source of carbon in biomass-based carbon. On the other hand, biomass-derived carbon has a high surface area, many micropores, and various functional groups, including carboxyl and hydroxyl, making it an abundant low-cost resource. The functional group can be modified by molecular grafting [31,33]. The reactivity of the carbon group is determined by the biomass type and the pyrolysis temperature. N-doping consists of pyrrolic N, pyridinic N, and graphitic N, with their formation process affected by the pyrolysis temperature [31].

Biomass-based carbon are palm empty fruit bunches, which contain high amounts of cellulose [31]. Prior studies have produced N-doped carbon material with high surface and active group of pyridinic N from biomass-derived carbon obtained from palm empty fruit bunches and a urea solution with the pyrolysis process for their potential applications in the energy sector, especially as electrocatalysts in oxygen reduction reactions in batteries [30–32,34,35]. While N-doped carbon from palm empty fruit bunches has been explored as an electrocatalyst, its performance as an adsorbent for Cr(VI) has not been previously investigated. N-doped carbon with pyridinic N active sites has the potential to absorb Cr(VI) metal. The pyridinic N form is affected by pH in acidic conditions, manifesting as protonated pyridinium N, which facilitates the adsorption process [36,37]. In the previous study, the manufacture of N-doped carbon based on palm empty fruit bunches has also been studied in its application as an electrocatalyst material for oxygen reduction reactions with pyridinic N active groups [30–32], but there has been no study of its application as a heavy metal adsorbent, Cr(VI). This work investigated the performance of N-doped carbon derived from empty palm

oil bunches in adsorbing the heavy metal Cr(VI) from aqueous solutions with a focus on adsorption kinetics.

2. Materials and Methods

2.1 Materials

Purchase of palm empty fruit bunches (PEFB) from PT Polytech Indonesia. Sodium hydroxide (NaOH), ethanol (99.9%), ammonia (NH_3 25%), iron (III) chloride ($FeCl_3.6H_2O$), potassium dichromate ($K_2Cr_2O_7$), and potassium hydrogen phthalate ($KHC_8H_4O_4$) were purchased from Merck. Urea ($(NH_2)_2CO$) purchased from PT Petrokimia Gresik. Hydrogen peroxide (H_2O_2 50%) and demineralized water were purchased from CV Hekto Gemilang Merak.

2.2 Methods

Synthesis Of N-Doped Carbon. Study of the synthesis process for N-doped aerogel production in previous studies [32]. The raw materials derived from cellulose, specifically palm empty fruit bunches, undergo a process of grinding and sieving to achieve a particle size of 150 mesh at a temperature of 100℃. The digestion of palm oil empty bunch powder was conducted using a 17.5% NaOH solution, with a volume of 20 mL allocated for each gram of the raw material powder. Chemical digestion is conducted through reflux at atmospheric pressure, maintaining a temperature of 100 ℃ for a duration of 2 h. The pulp produced in the subsequent phase of digestion undergoes filtration and is rinsed with demineralized water until the filtrate attains a clear hue. Subsequently, the pulp undergoes a drying process in the oven for four hours at a temperature of 101℃, followed by bleaching with a 3% H_2O_2 solution at 90℃ for one hour. For each gram of dry pulp powder, an application of 20 mL of 3% hydrogen peroxide is necessary. The cellulose pulp is generated from the bleaching phase, subsequently undergoing filtration and washing with demineralized water until achieving a neutral pH, which corresponds to that of the demineralized water itself. The pulp is subsequently combined with a cooled solution of cellulose cross-linker, maintained at –12℃ for a duration of 10 minutes. This solution consists of urea–NaOH–NH_4OH, incorporating 10 mL of water, 1 g of NaOH, 7.8 mL of NH_4OH (25% NH_3), and 4 g of urea. The pulp is combined with the cross-linking mixture through a stirring process lasting 30 min at a velocity of 200 revolutions per minute. The mixture is subsequently subjected to a cooling process at a temperature of –12 ℃ for a duration of 24 h to facilitate the gelation stage. The gel is maintained at room temperature for one hour, after which 15 mL of 96% ethanol is incorporated into the mixture. It was permitted to remain undisturbed for a duration of 24 h during the coagulation phase. Phases undertaken in the process of solvent exchange utilizing demineralized water. The resultant gel is subsequently subjected to cooling at a temperature of –20 ℃ for a duration of 24 h, followed by a freeze-drying process lasting 24 h at –40 ℃. Upon the process of freeze-drying, one acquires cellulose aerogel. We synthesize carbon by using cellulose aerogels. Pyrolysis

was performed in a nitrogen atmosphere, initiating with a 15-min purging of gas within the container. This stage was succeeded by a heating phase at 150°C for 30 min to facilitate moisture removal, followed by an elevation to 400°C for 30 min to achieve cellulose decomposition. The process culminated in a pyrolysis phase at 700°C for 2 h to produce N-doped carbon.

The analysis of functional groups within the material was conducted utilizing Fourier Transform Infrared Spectroscopy (FTIR; Thermo Scientific Nicolet iS10) across the wavenumber range of 4,000–400 cm^{-1}. The atomic composition of the samples was examined through Energy Dispersive X-ray Spectroscopy (EDS, AMETEK EDAX). The analysis of crystallinity in the material was conducted through X-Ray Diffraction (XRD; PANalytical, X'pert Pro) spectra, specifically within the 2θ angle range of 20-80°. The analysis of the material's surface area was conducted utilizing a nitrogen gas adsorption-desorption instrument (Nova 1200, Quantachrome) employing the BET (Brunauer-Emmett-Teller) method. Initially, the sample underwent pretreatment through heating at 300°C for a duration of 3 h in the presence of a flow of N_2 gas.

Adsorption of Cr(VI) Metal by N-Doped Carbon Adsorbent. Study 10 mg of nitrogen-doped carbon material synthesized on urea mass variation was applied to 50 mL plastic containers. Using 20 mL of a 100 ppm solution of Cr(VI) from K2Cr2O7 with pH 6 and adsorption durations of 10, 20, 30, 40, 50, 60, 90, and 120 min, each adsorption procedure was conducted in a batch system. Following the adsorption process, the amount of metal Cr adsorbed was measured using an atomic absorption spectrophotometer (AAS, Perkin Elmer AA 3110) to characterize the filtrate. Evaluation of the quantity of adsorbate retained with the formula [38] :

$$\mathrm{qe} = \frac{(\mathrm{Ci} - \mathrm{Ce})\ x\ V}{m} \tag{1}$$

Accompanied by the subsequent elucidation: qe represents the quantity of adsorbate that has been adsorbed (mg/g). Ci denotes the initial concentration of adsorbate ions (mg/L). Ce indicates the concentration of the remaining adsorbate ions at equilibrium (mg/L). V refers to the volume of the adsorbate (L), while m signifies the mass of the adsorbent (g).

The assessment of adsorption kinetics relies on the value of R nearing one in the graph depicting the variation of adsorption time. The order of adsorption reactions includes Pseudo-Zero, First, and Second-Order reactions, with the subsequent details[39]:

Pseudo-zero-order reaction formula:

$$q_e - q_t = k.t \tag{2}$$

Pseudo- first-order reaction formula:

$$\ln (q_e - q_{t)} = -k.t + \ln q_e \tag{3}$$

Pseudo-second-order reaction formula:

$$\frac{t}{q_t} = \frac{t}{q_e} + \frac{1}{kq_e^2} \tag{4}$$

In this context, qe represents the quantity of adsorbate that has been adsorbed at equilibrium, measured in milligrams per gram (mg/g). The variable qt denotes the

amount of adsorbate that has been adsorbed at a particular time t, also expressed in mg/g. The parameter k refers to the constant associated with the rate of adsorption, while t indicates the elapsed time, measured in minutes. The determination of reaction order is based on identifying the R^2 value that is nearest to 1.

3. Results and Discussion

According to material type analysis on the XRD pattern displayed in Figure 1, N-doped carbon has been effectively synthesized from empty fruit bunches of oil palm using a cross-linker solution of ammonia, urea, and NaOH through the processes of freeze-drying and pyrolysis. The cellulose aerogel made from oil palm empty fruit bunches by freeze-drying shows distinctive peaks at the (110) and (020) planes with 2θ angles of 20.28° and 22.09°, respectively, according to the XRD pattern shown in Figure 1(a). Following the pyrolysis of the cellulose aerogel, a new XRD pattern was created, as shown in Figure 1(b), which included distinctive peaks of amorphous carbon with the (002) plane index at an angle of 23.76°. This suggests the effective synthesis of N-doped carbon aerogel. The findings of the FTIR spectral study, which are further described in Figure 2, corroborate this.

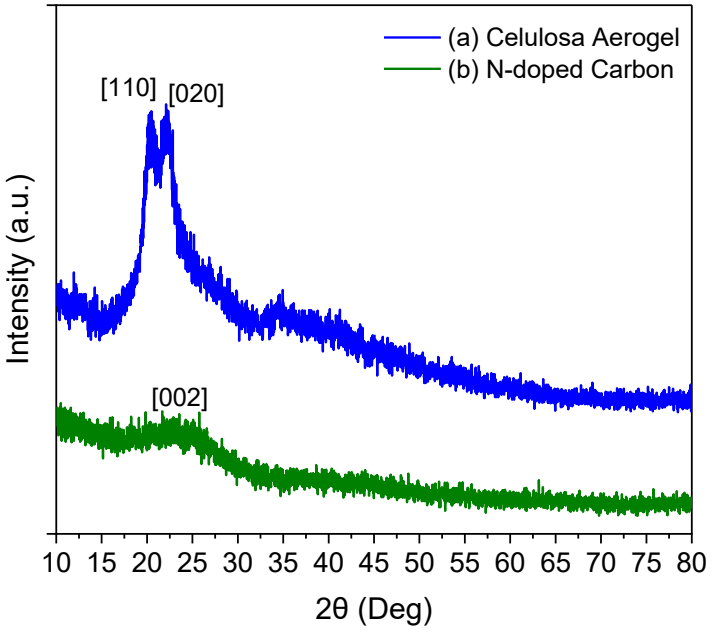

Fig. 1. The XRD patterns of the cellulose aerogel prior to pyrolysis and the XRD patterns of N-doped carbon following pyrolysis.

The FTIR spectra in Figure 2a indicate that the cellulose aerogel exhibits spectral absorption peaks at wavenumbers 1010 cm^{-1} (C-O), 1451 cm^{-1} (-CH_2-), 2847-2918

cm^{-1} (symmetric and asymmetric C-H bending), and 3367 cm^{-1} (O-H bond), which are indicative of cellulose. Moreover, spectral absorption peaks are observed at wavenumbers 1366 cm^{-1} (C-N), 1658 cm^{-1} (C=O), 1615 cm^{-1}, and 3196 cm^{-1} (N-H), which are indicative of urea as the crosslinker linking the cellulose chains. Figure 2(b) illustrates the FTIR spectra of N-doped carbon aerogels, characterized by the emergence of absorption peaks at wavenumbers 625-850 cm^{-1} and 2954 cm^{-1} (aromatic C-H), 1366 cm^{-1} (C-N), 1451 cm^{-1} (-CH_2-), and 1772 cm^{-1} (C=N), which are indicative of pyridinic N-type N-doping. This signifies that nitrogen-doped carbon aerogels containing pyridinic nitrogen functional groups have been effectively generated using the pyrolysis of cellulose aerogels derived from palm empty fruit bunches, utilizing ammonia, urea, and sodium hydroxide as crosslinking agents. The N-doping content was subsequently examined utilizing SEM-EDS, as illustrated in Figure 3.

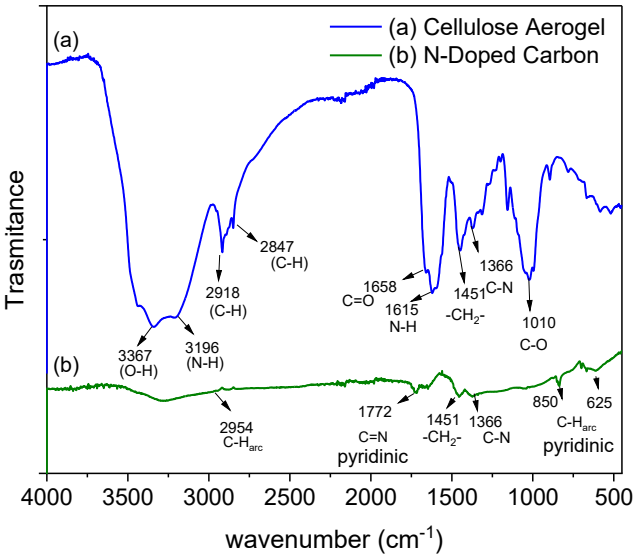

Fig. 2. FTIR spectra of nitrogen-doped carbon post-pyrolysis and the source of the cellulose aerogel pre-pyrolysis.

Figure 3 illustrates the distribution of carbon (C), oxygen (O), and nitrogen (N) atoms in nitrogen-doped carbon, exhibiting a homogeneous composition with atomic percentages of 51% for C, 36% for O, and 13% for N, respectively. This signifies that N-doped carbon has been effectively produced with a nitrogen doping level of 13%. Additional characterization was performed by evaluating the samples to ascertain the specific surface area utilizing the BET method, as illustrated in Figure 4 and Tabel 1. The findings demonstrate that cellulose aerogel possesses a specific surface area of 129 m^2/g, which significantly escalated to 3335 m^2/g following pyrolysis to produce N-

doped carbon. The produced N-doped carbon material was further evaluated for its efficacy as an adsorbent for Cr(VI) metal ions from a synthetic $K_2Cr_2O_7$ waste solution, as elaborated in Figure 5.

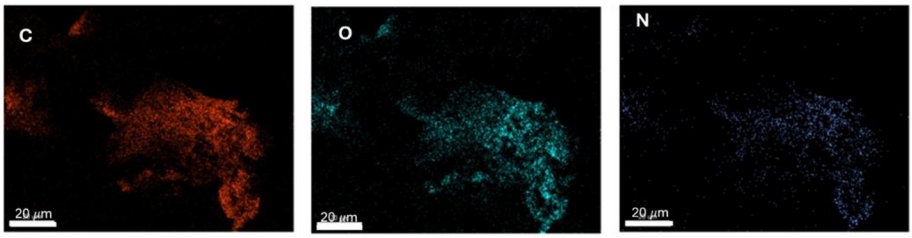

Fig. 3. A Distribution of carbon, nitrogen, and oxygen atoms in nitrogen-doped carbon**.**

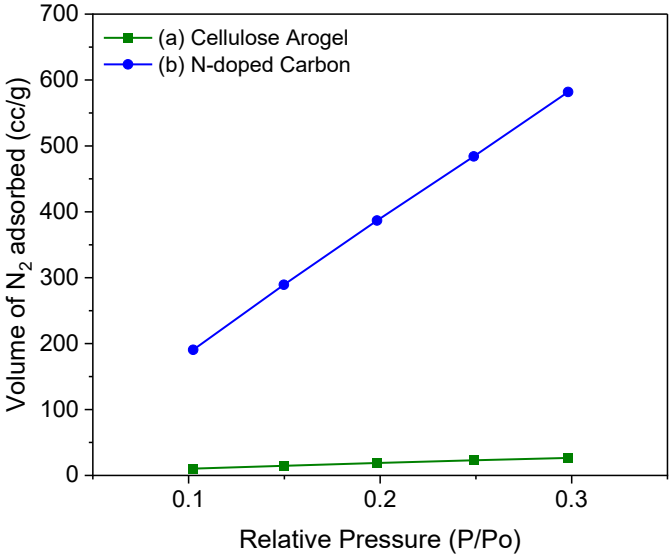

Fig. 4. Adsorption profile of N_2 gas on N-doped carbon samples post-pyrolysis and the source of cellulose aerogel prior to pyrolysis.

Table 1. Specific Surface Area of Cellulose Aerogel and N-Doped Carbon.

Sample	Specific Surface Area (m^2/g)
Cellulose Aerogel	129
N-Doped Carbon	3335

Figure 5 illustrates the quantity of Cr(VI) adsorbate at different adsorption contact durations (10, 30, 45, 60, 90, and 120 minutes), demonstrating that the amount of Cr(VI) increases until 30 minutes of contact time, after which it declines until 120 minutes. Following a contact duration of 30 minutes, the desorption of Cr(VI) ions adsorbed by N-doped carbon commenced. This signifies that the effective adsorption contact duration is 30 minutes, with an adsorption capacity of 126.05 mg of adsorbate per gram of adsorbent. An adsorption kinetics analysis was subsequently conducted utilizing the graphical method illustrated in Figure 5. The reaction kinetics analysis indicates that the graph with the R^2 value nearest to 1 corresponds to a pseudo-second-order reaction. This signifies that adsorption transpires by chemical contact. At pH 6, electrostatic interactions can occur between positively charged pyridinic nitrogen groups (Pyridinium N) on N-doped carbon adsorbents and negatively charged Cr(VI) ions, namely in the form of $(CrO_4)^{2-}$, as illustrated in Figure 7. At pH 6 (acidic circumstances), pyridinic nitrogen is present as the positively charged pyridinium ion, whilst Cr(VI) ions transition from the dichromate ion $(Cr_2O_7)^{2-}$ to the chromate ion $(CrO_4)^{2-}$ [25,40,41].

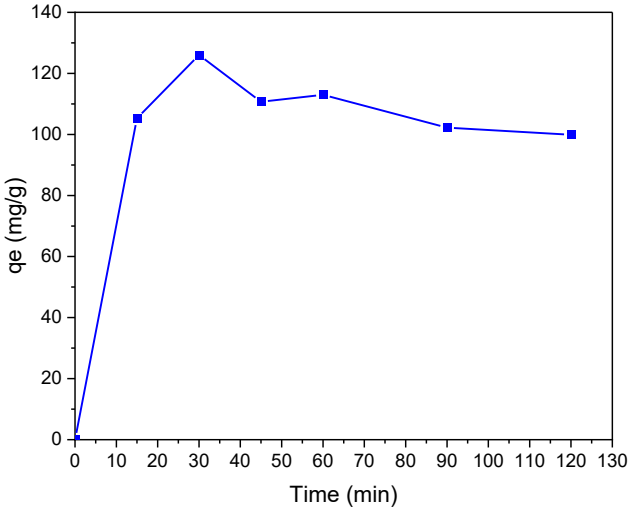

Fig. 5. Amount of Cr(VI) adsorbate adsorbed at different adsorption contact times.

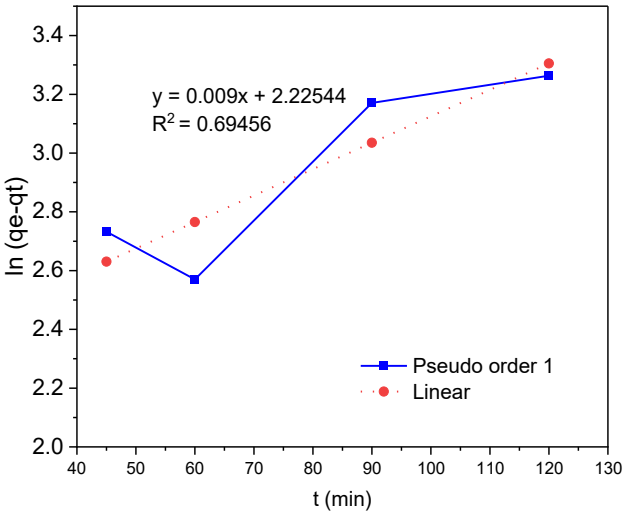

(a)

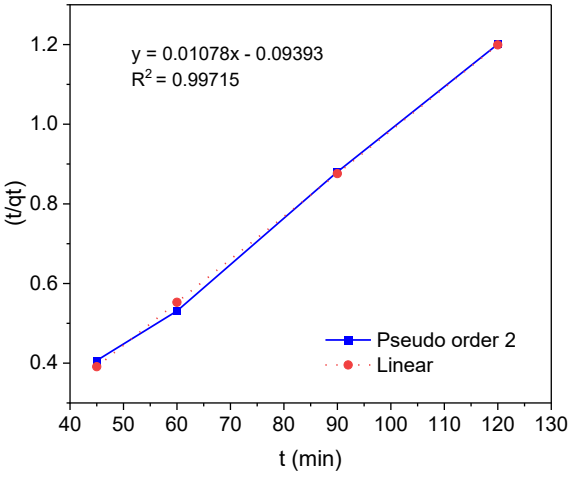

(b)

Fig. 6. Determination of reaction kinetics in the adsorption of N-doped carbon on Cr(VI): (a) 1st order, and (b) 2nd order.

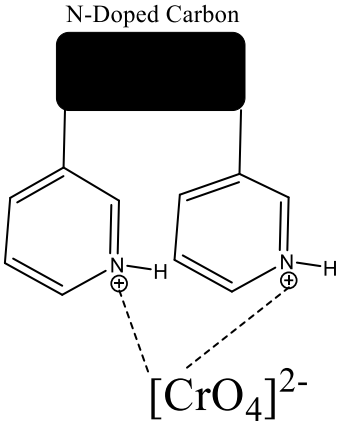

Fig. 7. Electrostatic chemical interaction between pyridinic N on N-doped carbon adsorbents and Cr(VI) ions at pH 6.

4. Conclusion

N-doped carbon has been effectively produced from cellulose aerogels derived from empty fruit bunches, achieving an N-doping percentage of 13% and an excellent specific surface area. Nitrogen-doped carbon containing pyridinic N absorbed Cr(VI) metal ions with a capacity of 126.05 mg/g, achieving optimal results at 30 min with an initial concentration of 100 ppm. The adsorption of nitrogen-doped carbon containing pyridinic N active groups and Cr(VI) metal ions as $(CrO_4)^{2-}$ species occurs through chemical interactions, with reaction kinetics adhering to pseudo-second-order kinetics.

Acknowledgments. We thank Ms. Lia Agustin, Mr. Iqbal Lintang Kusuma, Mr. Handoko Desta Priadi, Mr. Mahhathir Muhammad and Mr. Agus Jalaluddin for their assistance with the experiments. This research was fully supported by Ministry of Higher Education, Science and Technology of the Republic of Indonesia through a Regular Fundamental Research Grant (Contract No039/C3/DT.05.00/PL/2025 and 11018/PL2.2/HK/2025

Disclosure of Interests. The authors declare no conflicts of interest.

References

1. Zou D, Nie D, Wang W, Xu Q, Nie G. Fabrication of a MoS2@PAN composite membrane for efficient removal of toxic Cr(VI). Desalination 2025;600:118460. https://doi.org/10.1016/j.desal.2024.118460.
2. Zhao L, Duan H, Liu Y, Wang Y, Li M, Li M. Long-term exposure of zebrafish (Danio rerio) to Cr(VI): Reproductive toxicity and neurotoxicity. Reg Stud Mar Sci 2024;74:103559. https://doi.org/10.1016/j.rsma.2024.103559.

3. Wang Q, Zhang C, Song J, Bamanu B, Zhao Y. Inhibitory mechanism of Cr(VI) on sulfur-based denitrification: Bio-toxicity, bio-electron characteristics, and microbial evolution. J Hazard Mater 2024;472:134447. https://doi.org/10.1016/j.jhazmat.2024.134447.
4. Tian G, He F, Li X, Hu S, Zhao X, Guo S, et al. Novel mechanistic insights into Cr(VI) and Cr(III) induced discrepancies of cellular toxicity and oxidative injury events in Eisenia fetida. Science of The Total Environment 2024;944:173970. https://doi.org/10.1016/j.scitotenv.2024.173970.
5. Nie G, Wang W, Nie D, Xu Q, Zhang Y, Liu F, et al. Rationally designed composite adsorptive membrane for Cr(VI) adsorption and reduction combined with Cr(III) sequestration. Desalination 2025;607:118806. https://doi.org/10.1016/j.desal.2025.118806.
6. Zou W, Zhou F, Zhang Z, Ruan Q, Zhou J, Li Z, et al. Unveiling the distinctive characterization and adsorption behaviors of MnFe2O4 hydrochar/pyrochar composites for Cr(VI) removal. J Environ Chem Eng 2025;13:116052. https://doi.org/10.1016/j.jece.2025.116052.
7. Yang Q, Wang H, Zhong Y, Lu G, Dang Z, Zhang L. Co-adsorption behaviors and mechanisms of Cd(II), Pb(II), and Cr(VI) on sodium dodecyl sulfate modified attapulgite clay-supported nano zero-valent iron: Competitive or synergistic effect? Environ Res 2025;271:121107. https://doi.org/10.1016/j.envres.2025.121107.
8. Mohamed IMA, Hossam G, Shaker AM, Nassr LAE. Surface functionalization of TiO2 nanoparticles with hydrophobic tridentate Schiff base for a promising photocatalytic reduction of toxic Cr(VI) in aqueous solutions. Ceram Int 2025. https://doi.org/10.1016/j.ceramint.2025.01.436.
9. Phan T-TH, Nguyen H-DP, Nguyen N-P, Nguyen H-N, Duong T-LH, Tran B-A, et al. Development of a bioreactor with an integrated non-dispersive infrared CO2 sensor for rapid and sensitive detection of Cr(VI) toxicity in water. J Hazard Mater 2025;486:137089. https://doi.org/10.1016/j.jhazmat.2025.137089.
10. adhao JS, Rathod N V, Rao A, Ghugare CD, Chavan SM, Kubade A V, et al. Efficient removal of toxic Cr(VI) ions from waste streams by a novel Fe3O4@Formaldhyde Urea resin composites. Sustainable Chemistry One World 2025:100045. https://doi.org/10.1016/j.scowo.2025.100045.
11. Wu H, Lv H, Yu Y, Du Y, Du D. Ammonium persulfate-triggered modified chitosan biochar for co-adsorption of Cr(VI) and tetracycline antibiotics: Behavior and mechanisms. Int J Biol Macromol 2025;311:143432. https://doi.org/10.1016/j.ijbiomac.2025.143432.
12. Zhao X, Liang H, Wang Z, Li D, Shen X, Xu X, et al. Preparation of N-doped cellulose-based hydrothermal carbon using a two-step hydrothermal induction assembly method for the efficient removal of Cr(VI) from wastewater. Environ Res 2023;219:115015. https://doi.org/10.1016/j.envres.2022.115015.
13. Lima L dos S, Fernandes EP, Novelli A, Costa LP da, Monteiro MDS, dos Santos MVQ, et al. Adsorption and ecotoxicology studies with aqueous solution of Cr(VI) ions using adsorbent materials derived from Inga edulis. Chemosphere 2025;378:144378. https://doi.org/10.1016/j.chemosphere.2025.144378.
14. Li P, Zhang D, Huang S, Wang Y, Guo X. Excellent catalytic performance toward room temperature reduction of Cr(VI) in water over Ni/N-doped carbon catalysts prepared

by sol-gel method in the range of 800–1000 °C. J Alloys Compd 2025;1012:178374. https://doi.org/10.1016/j.jallcom.2024.178374.
15. He Y, Alhassan SI, Zhang W, Hou L, Chen X, Li X, et al. Electrochemically-mediated capture and reduction of Cr(VI) by highly porous N-doped carbon spheres. J Environ Chem Eng 2021;9:106067. https://doi.org/10.1016/j.jece.2021.106067.
16. Shah S, Mubeen I, Pervaiz E, Nasir H, Ahsan S, Saeed A, et al. Surface engineering of Ti3C2Tx MXenes for high-performance adsorption of toxic Cr(VI) contaminant vis-a-vis pristine MXenes. Mater Chem Phys 2025;334:130442. https://doi.org/10.1016/j.matchemphys.2025.130442.
17. Sharma P, Monisha B, Kumar PS, Krishnaswamy VG, Rangasamy G. Effective removal of toxic mixed azo dyes and Cr (VI) ions from wastewater using an integrated approach. Desalination Water Treat 2024;320:100654. https://doi.org/10.1016/j.dwt.2024.100654.
18. Susanto S, Prasdiantika R. Adsorption of Chromium (VI) with Silica Coated on Iron Sand Magnetic Material Modified with Propyldiethylenetriamine. Jurnal Teknik Kimia Dan Lingkungan 2024;8:70–81. https://doi.org/10.33795/jtkl.v8i2.5478.
19. Wang Y, Chen Y, Shan F, Zhang T, Zhang Z, Liu M. L-glutamic acid-functionalized graphene oxide with characteristic of anti-stacking towards efficient adsorption-reduction removal of Cr(VI). J Environ Chem Eng 2024;12:114764. https://doi.org/10.1016/j.jece.2024.114764.
20. Liu H, Zhang F, Peng Z. Adsorption mechanism of Cr(VI) onto GO/PAMAMs composites. Sci Rep 2019;9:3663. https://doi.org/10.1038/s41598-019-40344-9.
21. Jia Z, Liang F, Xu X, Zhou H, Zhang Y, Liang P. One-pot amination and carboxylation functionalization of lignin for efficient adsorption of Cr(VI) and Cd(II): Influence of functional groups on adsorption equilibrium and mechanism. Colloids Surf A Physicochem Eng Asp 2024;703:135278. https://doi.org/10.1016/j.colsurfa.2024.135278.
22. Bibbly A, Mercier L. Mercury(II) ion adsorption behavior in thiol-functionalized mesoporous silica microspheres. Chem Mater 2002;14:1591.
23. Siwalima V, Philip JYN, Nobert J. Synthesis of N-doped multi-walled carbon nanotubes derived from plastic waste for adsorption of Pb2+ ions in aqueous solutions. Diam Relat Mater 2025;155:112266. https://doi.org/10.1016/j.diamond.2025.112266.
24. Wang C, Lin G, Zhao J, Wang S, Zhang L. Enhancing Au(III) adsorption capacity and selectivity via engineering MOF with mercapto-1,3,4-thiadiazole. Chemical Engineering Journal 2020;388:124221. https://doi.org/10.1016/j.cej.2020.124221.
25. Zhang H, Luo L, Zhao Z, Shen Y, Cui J, Shi X, et al. Enhanced SO2, NO, and Cr (VI) removal by lignin-derived high N-doped activated carbon through one-pot strategy: Structure development, structure–performance relationship and mechanism insight. Sep Purif Technol 2024;348:127687. https://doi.org/10.1016/j.seppur.2024.127687.
26. Sun X, Peng Q, Wang Z, Li C, Huang Y. N-doped porous carbon derived from Cr-tanned leather shaving wastes for synergetic adsorption of Cr(VI) from aqueous solution. Mater Lett 2021;284:128815. https://doi.org/10.1016/j.matlet.2020.128815.
27. Lv Z, Chen W, Cai Y, Chen K, Li K, Fang M, et al. Homogeneous Ni nanoparticles anchored on mesoporous N-doped carbon as highly efficient catalysts for Cr(VI), tetracycline and dyes reduction. Appl Surf Sci 2022;575:151748. https://doi.org/10.1016/j.apsusc.2021.151748.

28. Guo W, Lei Y, Yu X, Wu Y. Ratiometric fluorometric and colorimetric dual-signal sensing platform for rapid analyzing Cr(VI), Ag(I) and HCHO in food and environmental samples based on N-doped carbon nanodots and o-phenylenediamine. Food Chem 2024;437:137945. https://doi.org/10.1016/j.foodchem.2023.137945.
29. Lan X, Gao B, Liu Z, Lin P, Liu H, Fu H, et al. Amine–functionalised magnetic graphene–oxide nanosheets for the adsorption and reduction of Cr(VI) in water. Diam Relat Mater 2025;152:111891. https://doi.org/10.1016/j.diamond.2024.111891.
30. Afifa UI, Susanto S, Setyawan H, Nurtono T, Widiyastuti W. Synthesis and Characterization of N-Doped Carbon Aerogel Based on Oil Palm Empty Fruit Bunch as Oxygen Reduction Reaction Electrocatalyst in Seawater Batteries. Key Eng Mater 2023;971:65–71. https://doi.org/10.4028/p-wd8ZXi.
31. Susanto S, Nurtono T, Widiyastuti W, Yeh M-H, Setyawan H. Controlling N-Doping Nature at Carbon Aerogels from Biomass for Enhanced Oxygen Reduction in Seawater Batteries. ACS Omega 2024;9:13994–4004. https://doi.org/10.1021/acsomega.3c09297.
32. Susanto S, Avabel N, Septianingrum N, Nurtono T, Setyawan H. N and Fe Doped-Carbon Aerogel for High Performance of Oxygen Reduction Reactions Electrocatalyst in Magnesium-Air Battery. Materials Science Forum 2024;1142:63–70.
33. Wang X, Xu J, Liu J, Liu J, Xia F, Wang C, et al. Mechanism of Cr(VI) removal by magnetic greigite/biochar composites. Science of The Total Environment 2020;700:134414. https://doi.org/10.1016/j.scitotenv.2019.134414.
34. Susanto S, Rochman TF, Kamandanu MR, Nurtono T, Widiyastuti W, Setyawan H. Synthesis of Metal-Free Carbon Aerogel with Nitrogen-Doped from Pyrolysis of Cellulose Aerogels Based on Coir Fibers Using Ammonia Urea System as Electrocatalyst of Oxygen Reduction Reaction for Cathode in Seawater Batteries. Key Eng Mater 2023;971:55–63. https://doi.org/10.4028/p-PC7nGO.
35. Wang G, Xu X, Kou X, Liu X, Dong X, Ma H, et al. N-Doping of Graphene Aerogel as a Multifunctional Air Cathode for Microbial Fuel Cells. ACS Appl Mater Interfaces 2021;13:51312–20. https://doi.org/10.1021/acsami.1c12605.
36. Ide K, Kunimoto M, Miyoshi K, Takano K, Matsuoka K, Homma T. Surface pH Effects on Catalytic Behavior of Pyridinic Nitrogen on Nitrogen-doped Carbon Nanotube in CO2 Electrochemical Reduction. Electrochemistry 2023;91. https://doi.org/10.5796/ELECTROCHEMISTRY.22-00134.
37. Rauf M, Zhao Y-D, Wang Y, Zheng Y, Chen C, Yang X-D, et al. Insight into the different ORR catalytic activity of Fe/N/C between acidic and alkaline media: Protonation of pyridinic nitrogen. Electrochem Commun 2016;73. https://doi.org/10.1016/j.elecom.2016.10.016.

38. Augustine A, Ishaq B, Akpomie T, Uche Augustine A, Akpomie TM, Odoh R. Removal of Lead (II) and Iron (II) ions from Aqueous Solutions Using Watermelon (Citrillus Lanatus) Peels as Adsorbent. J Chem 2019;3:1–7.
39. Ulfa M, Solikah AA, Fadhilah ZA, Setiarini I, Syadida ZQ. Studi Optimisasi dan Kinetika Adsorpsi Silika dari Lumpur Lapindo dengan Metode Sol-Gel Menggunakan P123-Putih Telur. ALCHEMY Jurnal Penelitian Kimia 2024;20:49–61. https://doi.org/10.20961/alchemy.20.1.75659.49-61.
40. Anthony E, Oladoja N. Process enhancing strategies for the reduction of Cr(VI) to Cr(III) via photocatalytic pathway. Environmental Science and Pollution Research 2022;29. https://doi.org/10.1007/s11356-021-17614-z.
41. Björkegren S, Karimi R, Martinelli A, Natesan J, Hashim M. A New Emulsion Liquid Membrane Based on a Palm Oil for the Extraction of Heavy Metals. Membranes (Basel) 2015;5:168–79. https://doi.org/10.3390/membranes5020168.